Int. J. Heat Mass Transfer. Vol. 24, No. 12, pp. 1925–1935, 1981.
Printed in Great Britain

0017-9310/81/12 1925-11 $02.00/0
Pergamon Press Ltd.

UNSTEADY INTERNAL BOUNDARY LAYER ANALYSIS APPLIED TO GUN BARREL WALL HEAT TRANSFER*

MICHAEL J. ADAMS† and HERMAN KRIER‡
University of Illinois at Urbana-Champaign, Urbana, Illinois, U.S.A.

(*Received* 29 *November* 1979 *and in revised form* 1 *June* 1981)

Abstract—Convective heating to gun barrel walls is of considerable importance when attempting to evaluate the degradation of performance in a ballistic device. The purpose of this study was to isolate and examine convective heating in order to calculate gun tube wall temperature as occurs during the firing of a projectile. Internal flow structure was decoupled by specifying inviscid core properties through measured and assumed axial and temporal variations. A fluid mechanics model was then used to solve the unsteady, compressible, and turbulent momentum and energy boundary layer development at discrete piston locations. Shear layer solutions were coupled through the energy equation. A consideration of radial heat conduction into the bore surface of the ballistic device was used to predict the interior wall temperature history at all locations behind a moving projectile. The results, when compared to those predictions which utilize integral methods and assumed known heat transfer coefficients, indicate that conventional integral methods do not adequately represent the convective heat transfer process. The influence of transverse curvature on the surface heating of small bore guns was examined. Recommendations are given for improving the present model.

NOMENCLATURE

a_p, piston acceleration;
A, turbulence damping coefficient;
b, average gas covolume;
c, coefficient $[\rho\mu/(\rho\mu)_e]$;
D, transformation constant $[=(L - L_0)(2\xi)^{1/2}]$;
C_p, gas specific heat;
d_p, penetration depth;
f, stream function;
G, total enthalpy ratio $[=H/H_e]$;
H, total enthalpy;
H_s, shape factor;
h, static enthalpy;
h_c, local heat transfer coefficient;
k_g, k_s, thermal conductivity (g = gas, s = solid);
k_2, turbulence constant;
l, turbulence mixing length;
L, piston displacement from breech;
L_0, initial piston displacement;
ΔL, incremental piston displacement;
$\dot{L}$, $dL/dt = U_p$;
P, P_0, P_b, gas pressure (0 = breech, b = base of piston);
Pr, Prandtl number;
Pr_t, turbulent Prandtl number;
q, local heat flux;
r_c, metric coefficient;
r_0, bore radius;
Re_l, Re_θ, Reynold's number base on L and θ respectively;
R_g, gas constant;
St, Stanton number;
t, time;
T_g, T_s, temperature (g = gas, s = bore surface);
u, axial gas velocity;
U_p, piston velocity;
x, y, Cartesian axial and normal coordinates;
Δx, axial grid spacing.

Greek symbols

α_D, thermal diffusivity $[=(\rho C_p/\mu)s]$;
Γ, turbulence intermittency factor;
γ, specific heat ratio;
δ, boundary layer thickness;
δ^*, boundary layer displacement thickness;
ε, eddy viscosity;
ε^+, eddy diffusivity $[=\rho\varepsilon/\mu]$;
η, transformed stream normal coordinate;
θ, boundary layer momentum thickness;
μ, gas viscosity;
ν, kinematic gas viscosity;
ξ, transformed axial coordinate;
ρ, gas density;
τ, shear stress.

Subscripts

0, initial or reference values;
i, n, axial grid index;
j, stream normal grid index;
e, boundary layer edge properties ($y = \delta$);
w, wall properties ($y = 0$).

Superscripts

$'$, derivative in η $(=\partial/\partial\eta)$;
$''$, perturbed quantity;
$\bar{\ }$, mean or average quantity.

*Work supported, in part, by US Army ARRADCOM, Dover, NJ, under contract No. DAAA 25-76-C0143.

†Research Associate; Presently: Scientist, The Aerospace Corporation, Ed Segundo, California.
‡Professor, Department of Mechanical and Industrial Engineering.

INTRODUCTION

EVERY internal ballistic device is designed in correspondence with a pressure-travel history which allows a projectile travelling within the device to attain a desired maximum velocity at the launch tube exit. Many factors can inhibit a ballistic device from attaining the performance prescribed by the system design [1]. A primary factor in this regard is erosion of the interior walls of the launch tube. Erosion acts within highly localized regions to increase the diameter of the launch tube. Tube degradation eventually allows the propelling gas to escape around the moving projectile. This leakage causes the maximum projectile velocity to decrease over repetitive cycles.

The extent to which each erosion source (mechanical, thermal, chemical or hydrodynamic) contributes to tube wear has not been resolved at this time [2]. However, experimental studies [3, 4] do suggest that a reduction of bore surface temperature during the ballistic event will delay the onset of tube erosion. Bore surface temperature measurement during a single ballistic event is difficult to obtain due to the extremely high heating rate and short action time associated with the event. Temperature measurements in a gun tube have been made and inner surface temperature estimates extrapolated from such data [4]. However, the studies were confined to one axial location and used a large diameter (105 mm) bore. Use of a similar experiment on small diameter (5.56 mm) systems is much more difficult. An alternative to the experimental approach is to develop an analytical model to examine bore surface heating. In response to that need, this study will isolate and examine, at least qualitatively, the process associated with convective surface heating in a ballistic device.

APPROACH

As shown in Fig. 1, a ballistic device in this study is idealized as a smooth, enclosed tube which incorporates a moving piston instead of a projectile. Unlike actual systems, the idealized system ignores processes associated with propellant combustion and instead views the propelling gas as a non-reacting, well mixed fluid. Furthermore, the idealized system ignores gas swirl effects which are induced in actual systems by projectile spin. The flow structure is represented as an attenuating, inviscid core coexisting with a growing turbulent, unsteady, and compressible boundary layer along the inner bore surface. Shear layer development depends on both the state of the layer (turbulent vs. laminar) and the temporal and spatial variations at points bounding the viscous layer. Turbulence transition can essentially be ignored since the ensuing flow exhibits very high Reynold's numbers quite early in the ballistic cycle. Coupling between the shear layer and the conditions along its boundaries can be eliminated using various simplifying assumptions.

The decoupling strategy used by this study is shown in Fig. 2. For a fixed piston location, one assumes that core conditions along the outer edge of the shear layer

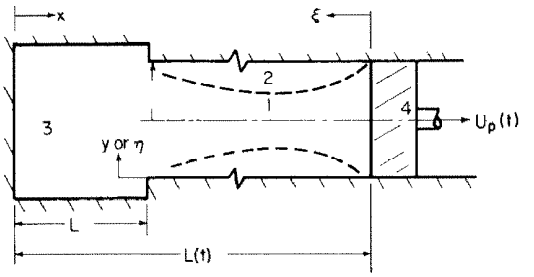

1 = Inviscid Core
2 = Turbulent, Compressible, Unsteady Boundary Layer
3 = Chamber
4 = Piston

FIG. 1. An idealized ballistic device.

can be specified prior to calculating boundary layer development. It is also assumed that the conditions along the inner edge of the shear layer are well represented using wall conditions prevailing prior to a boundary calculation. Unsteady boundary layer development is thus viewed through discrete piston displacements somewhat like flash pictures. Discrete boundary layer solutions (corresponding to a fixed piston location) provide local heat flux information at predetermined axial locations along the bore. Locally, this heat flux information specifies an energy balance at the wall/gas interface which provides for a solution to an unsteady radial heat conduction problem. This solution in turn yields an updated surface temperature at each axial location.

Though the analysis views unsteady boundary layer development by discrete piston displacements, in the limit of small displacements, the proposed discrete analysis should yield reasonable results closely approximating those results from a more exact computational treatment of the fully coupled problem.

In the present study, the unsteady derivatives ($\partial/\partial t$) of the governing shear layer equations are rewritten in terms of piston displacement ($\dot{L}\partial/\partial L$). Successive boundary layer solutions are coupled by numerical differentiation. The derivatives will now reflect the flow history calculated on previous piston displacements. Initially the boundary layer is viewed as being timewise and streamwise similar, i.e. $\partial/\partial x$, $\partial/\partial L = 0$. On subsequent piston displacement, the boundary layer is viewed as timewise similar at all new axial locations uncovered by the piston motion. Each incremental displacement is restricted to uncover only one new axial location.

INVISCID CORE MODEL

The inviscid core sets the outer boundary conditions for each shear layer solution. For this study, streamwise variations of core flow parameters are represented by functional relationships derived from a simple Lagrange ballistic model [1]. These relationships are listed in Table 1. The Lagrange model assumes that the

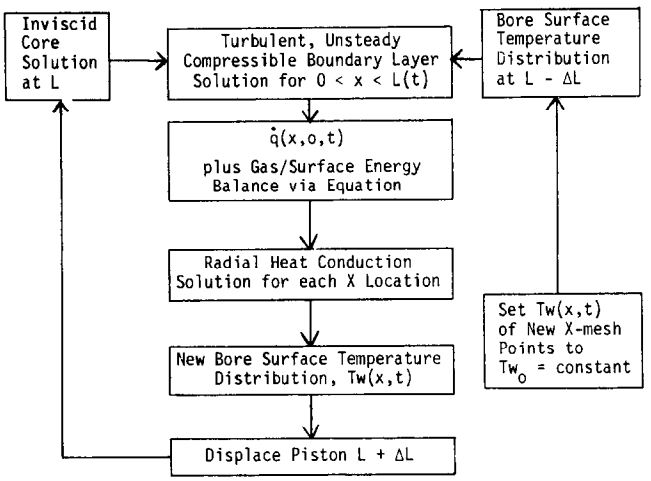

FIG. 2. Decoupling sequence.

Table 1. Inviscid core approximation: streamwise variations

	Lagrange
Axial velocity	$u_e = u_p \frac{x}{L}$
Axial pressure gradient	$\frac{\partial P_e}{\partial x} = -\rho_e \frac{x a_p}{L}$
Gas density	$\rho_e = \frac{M_0^*}{L}$
Gas temperature	$T_e(x) = P_e(1/\rho_e - b)/R_g$
Gas pressure	$P_e(x) = \int_{x_i}^{x} \frac{\partial P}{\partial x} dx$

* M_0 = reference mass of gas/unit cross-sectional area.

density of the propelling gas is constant over a fixed spatial domain. This assumption implies the existence of a linear velocity and parabolic pressure distribution in the gas behind the piston. The model imposes a constant ratio ($\neq 1$) of breech/piston base pressure for all time, a condition obviously in error before piston motion begins. However, the Lagrange model is representative of prevailing conditions in the inviscid core for later times in a ballistic cycle [5]. The exactness of the core flow representation will obviously determine the precision of the boundary layer solutions of the present study. Since the Lagrange model is a simplified core flow model, results from ensuing shear layer solutions must be viewed on a qualitative basis. More rigorous core flow models, such as that of Tuckmantel and Chou [6] or Buckingham [7], would help to remove this restriction. Such models would have been employed had they been available to the present study.

The Buckingham model has been patched at selected time intervals to a modified boundary layer integral matrix procedure of Kendall and Bartlett [8]. Patching is done by matching conditions associated with core turbulence, entropy and concentration gradients, as well as the usual edge velocity and pressure conditions. The model also considers wall surface erosion through finite rate gas kinetics in the boundary layer solution. However, the model does not appear to couple transient heating of the bore surface with shear layer development. Hence this model deals primarily with the erosion mechanisms associated with gas to surface chemical interaction, certainly an important component of the overall erosion problem. The present study assumes a non-reacting boundary layer and a simplified turbulence consideration, thereby restricting the investigation to the convective heating process.

Using a less rigorous treatment of turbulent boundary layer development, Anderson and Dahm [9] employ an approximate integral analysis procedure. With various approximations, an integral analysis provides a differential equation in momentum thickness, $\theta(x, t)$ which in turn can be solved by various numerical methods. After solving for the momentum thickness, one can obtain local quantities of interest (wall shear and heat flux) by imposing other approximations (Reynolds and Colburn analogies). Specifically, the Chilton–Colburn analogy eliminates the need to solve the unsteady, boundary layer energy equation. Anderson and Dahm [9] conducted their analysis for two limiting classes of operation, namely the "constant base pressure" and "simple wave" systems. Similar to the present study, these two limiting cases also constitute assumptions on inviscid core behavior.

Though an integral analysis presents significant computing time and cost savings, the validity of using Reynolds and Colburn analogies in a ballistic environment can be questioned. The present study suggests that these approximations may not be representative of the processes associated with a ballistic system.

TURBULENT BOUNDARY LAYER MODEL

The conservation equations for an unsteady, turbulent, and compressible boundary layer are written as follows.

Conservation equations

Mass

$$\frac{\partial}{\partial t}(\rho r_c) + \frac{\partial}{\partial x}(\rho u r_c) + \frac{\partial}{\partial y}(\overline{\rho v} r_c) = 0 \tag{1}$$

where

$$r_c = r_0 - y.$$

Streamwise momentum

$$\rho\frac{\partial u}{\partial t} + \rho u\frac{\partial u}{\partial x} + \overline{\rho v}\frac{\partial u}{\partial y} = -\frac{\partial p}{\partial x} + \frac{1}{r_c}\frac{\partial}{\partial y}(r_c\tau) \tag{2}$$

where

$$\frac{\tau}{\rho} = \nu\frac{\partial u}{\partial y} - \overline{u''v''}, \quad \overline{\rho v} = \overline{(\rho + \rho'')(v + v'')}.$$

Streamwise energy

$$\rho\frac{\partial H}{\partial t} + \rho u\frac{\partial H}{\partial x} + \overline{\rho v}\frac{\partial H}{\partial y} = \frac{\partial p}{\partial t} + \frac{1}{r_c}\frac{\partial}{\partial y}[r_c(q + u\tau)] \tag{3}$$

where

$$q = k_g\frac{\partial h}{\partial y} - \overline{\rho v''h''},$$

$$(q + u\tau) = \frac{\mu}{Pr}\frac{\partial H}{\partial y} - \overline{\rho v''H''} + \mu\left(1 - \frac{1}{Pr}\right)u\frac{\partial u}{\partial y} - \overline{\rho u v''v''},$$

$$H = h + \frac{u^2}{2}.$$

State (Nobel–Abel)

$$P\left(\frac{1}{\rho} - b\right) = R_g T. \tag{4}$$

Equations (1)–(3) use a variable r_c to transfer the flow field coordinate system from the actual flow axis to the bore surface. The variable r_c represents the normal distance from a point along the flow axis to a point within the boundary layer that is measured perpendicular to the internal contour of the surface. For the geometry of this study $r_c = r_0 - y$. Essentially, transverse curvature is considered through the variable r_c. Note that for a large bore radius, $r_c \simeq r_0$ or a thin shear layer, equations (1)–(3) assume the expected planar form.

The boundary conditions for this study are written as follows:

Wall conditions ($y = 0$)

$$u(x,t) = 0, \quad \text{(no slip)} \tag{5a}$$

$$v(x,t) = 0, \quad \text{(no mass transfer)} \tag{5b}$$

$$H(x,t) = h_w(x,t) = \bar{C}_p T_w(x, t-1). \quad \text{(surface coupling)} \tag{5c}$$

Edge conditions ($y = \delta$)

$$u(x,t) = u_p\frac{X}{L}, \quad \text{(see Table 1)} \tag{5d}$$

$$v(x,t) = 0,$$

$$H(x,t) = \bar{C}_p T_e(x,t) + Pb + (U_p X)^2/2L^2. \tag{5f}$$

Note that equation (5f) reflects the use of equation (4), a high pressure consideration.

The dimensional equations (1)–(3) are rewritten using coordinate transformations suggested by Bartlett *et al.* [10], namely:

Axial $$\xi = -\ln(X/L). \tag{6a}$$

Stream normal $$\eta = D^{-1}\int_0^y \left(\frac{r_c}{r_0}\right)\frac{\rho}{\rho_e}\mathrm{d}y, \tag{6b}$$

where $$D = (L - L_0)(2\xi)^{1/2}.$$

The variable ξ increases from zero at the piston base ($X = L$) to infinity at the breech ($X = 0$). The finite axial domain $L > X > 0$ is now transformed to a semi-infinite domain $0 < \xi < \infty$. In the transformed coordinate system, one no longer needs to deal with the breech, an area of discontinuous flow interactions. The transformed space supports a unidirectional march from a vicinity near the piston base towards but never to the breech. The singularity at the piston/bore interface is avoided by starting all computations a small distance away from the piston base. The required stand-off distance follows those restrictions governing any leading edge problem.

Equations (1) and (2) are combined by the stream function, f, defined as follows:

$$f - f_w = \frac{1}{D}\int_0^y \left(\frac{r_c}{r_0}\right)\frac{\rho u}{\rho_e u_e}\mathrm{d}y = \int_0^{\eta'}\frac{u}{u_e}\mathrm{d}\eta, \tag{7a}$$

where

$$f_w = \frac{1}{D}\int_0^\xi \frac{(\rho V)_{y=0}}{\rho_e u_e}\mathrm{d}\xi = 0 \tag{7b}$$

by equation (5b).

For simplicity, this study uses a two-region mixing length model to represent flow turbulence. The relationship for the inner eddy viscosity value was suggested by Van Driest [11] while the expression for the outer region was proposed by Klebanoff [12]. These expressions are written as:

Eddy viscosity

Inner region $$\varepsilon_i = l^2\left|\frac{\partial u}{\partial y}\right|.$$

Outer region $$\varepsilon_0 = k_2 U_e \delta^* \Gamma,$$

where $$l = 0.4y[1 - \exp(-y/A)],$$

$$A = 26\nu\left\{\frac{\tau_w}{\rho}\right\}^{1/2},$$

$$\Gamma = [1 + 5.5(y/\delta)^6]^{-1}.$$

The mixing length approach models Reynolds stress in terms of mean flow parameters thus implicitly defining the Reynolds stress transport. The functional relationships between the turbulence quantities of eddy viscosity and eddy conductivity are related by a new parameter, the turbulent Prandtl number Pr_t. The turbulent Prandtl number allows eddy viscosity to represent the primary turbulent quantity of interest. As in other studies [10, 13], the turbulent Prandtl number is assumed to be constant, $Pr_t = 0.9$.

High pressure relationships for viscosity and thermal conductivity are not easily formulated. Theoretical expressions based upon statistical considerations can be applied. However, the present study uses simplified expressions to represent bulk transport properties, namely

$$\left(\frac{\mu}{\mu_0}\right) = \left(\frac{T}{T_0}\right)^{0.4} \quad \text{and} \quad \left(\frac{k}{k_0}\right) = \left(\frac{T}{T_0}\right)^{0.5} \tag{4b, 4c}$$

The transformed conservations can now be written following the proposed coordinate transformations and restrictive core flow and turbulence assumptions.

Transformed conservation equations

Momentum

$$\left[\frac{C}{Re_L}(1+\varepsilon^+)\left(\frac{r_c}{r_0}\right)^2 f''\right]' - \frac{(2\xi)(L-L_0)\dot{L}}{Lu_p}\left[\left(\frac{\partial f'}{\partial \xi} - f'\right)\right.$$
$$\left. - \eta\left(\frac{1}{2\xi} + \frac{L_0}{L-L_0}\right)f'' + \frac{1}{L}\left(\frac{\partial f'}{\partial L} + \frac{f'}{U_p}\frac{\partial U_p}{\partial L}\right)\right]$$
$$- f'\frac{(2\xi)(L-L_0)}{L}\left(\frac{\partial f'}{\partial \xi} - f'\right) - f''\frac{(2\xi)(L-L_0)}{L}$$
$$\times\left[f\left(\frac{1}{2\xi} - 1\right) + \frac{\partial f}{\partial \xi}\right] + \frac{(2\xi)(L-L_0)}{\rho_e u_e^2}\frac{\partial P}{\partial \xi} = 0. \tag{8}$$

Energy

$$\left[\frac{C}{Re_L Pr}\left(1 + \frac{\varepsilon^+ Pr}{Pr_t}\right)\left(\frac{r_c}{r_0}\right)^2 G'\right]' + \left\{\frac{C}{Re_L P_L}\left[(Pr-1)\right.\right.$$
$$\left.\left. + \frac{\varepsilon^+ Pr}{Pr_t}(Pr_t - 1)\right]\frac{u_e^2 f' f''}{H_e}\right\} - \frac{2\xi(L-L_0)\dot{L}}{Lu_p}$$
$$\times\left[\frac{\partial G}{\partial \xi} - \eta\left(\frac{1}{2\xi} + \frac{L_0}{L-L_0}\right)G' + L\frac{\partial G}{\partial L}\right]$$
$$- f'\frac{(2\xi)(L-L_0)}{L}\frac{\partial G}{\partial \xi} + \frac{2\xi(L-L_0)}{L}$$
$$\times\left[f\left(\frac{1}{2\xi} - 1\right) + \frac{\partial f}{\partial \xi}\right]G' + \frac{2\xi(L-L_0)\dot{L}}{H_e L u_p}$$
$$\times\left(\frac{1}{L}\frac{\partial P}{\partial \xi} + \frac{\partial P}{\partial L}\right) = 0, \tag{9}$$

where

$$Re_L = \frac{\rho_e U_p (L-L_0)}{\mu_e}, \quad C = \frac{\rho\mu}{\rho_e\mu_e}, \quad G = \frac{H}{H_e}, \quad \varepsilon^+ = \frac{\rho\varepsilon}{\mu}.$$

Boundary conditions

Wall conditions ($\eta = 0$)

$$f' = 0, \quad G = C_p T_w/[C_p T_s + Pb + (U_p X)^2/2L^2]. \tag{10a}$$

Edge conditions ($\eta = \delta$)

$$f' = 1, \quad G = 1. \tag{10b}$$

With reference to Fig. 1, an implicit stepwise marching procedure is employed to obtain boundary layer solutions in the direction of increasing ξ. The numerical procedures used to obtain shear layer solutions are those procedures used by Cebeci *et al.* [13] but extended to include time dependence. Briefly, the numerical strategy proceeds as follows. At a given axial location, streamwise (ξ) and timewise (now L) partial derivatives in equations (8) and (9) are discretized using three- and two-point difference formulae respectively. The resulting ordinary differential equations are then rewritten using Lagrange interpolation formulae to replace stream normal (η) derivatives. A variable (geometric) grid spacing is employed in the η = constant plane while a constant grid spacing is employed for the ξ, L = constant planes. At each axial location, equations (8) and (9) now represent a set of N algebraic equations in $N-2$ unknowns. These equation sets can be written in the general matrix form

$$A_{ij}x_i = b_i. \quad i = 1,\ldots,N;\ j = 1,\ldots,N. \tag{11}$$

With the boundary conditions of equation (10), equation (11) is solved for all x_i values using a simple block elimination method [14]. Higher order derivatives at each η-location are calculated by reintroducing x_i values into the previously used interpolation formulae.

The computational strategy at a given axial location proceeds as follows. As an initial guess one assumes both a linear velocity and static enthalpy profile across the boundary layer. Turbulence and fluid properties, calculated from these assumed profiles, linearize the momentum equation which is then solved to obtain a new velocity profile estimate. This estimate along with previously calculated turbulence and fluid property values are used to solve the energy equation. This solution yields a new gas temperature profile which in turn provides a new static enthalpy profile estimate. Sequential iteration between the momentum and energy equations continues until convergence is observed in both the wall shear (f''_w) and displacement thickness (δ^*) values.

Radial heat conduction model

For sufficiently large piston acceleration and no preheating of the bore surface, the effects of axial heat conduction can be neglected. Using this assumption, the heat equation for any annular region along the bore becomes

$$\frac{\partial T_s}{\partial t} = \alpha_D \frac{1}{r} \frac{\partial}{\partial r}\left(r \frac{\partial T_s}{\partial r}\right) \tag{12}$$

where α_D = thermal diffusivity of the bore material. A solution of equation (12) requires two boundary conditions. The boundary conditions for this study are:

Inner ($r = r_0$),

$$-k_g \frac{\partial T}{\partial r} = -k_s \frac{\partial T_s}{\partial r}; \tag{13a}$$

Outer ($r = r_0 + d_p$),

$$-k_s \frac{\partial T_s}{\partial r} = 0. \tag{13b}$$

Equation (13a) exhibits the coupling to the boundary layer solution. Equation (13b) implies relaxation of the temperature into the bore to some ambient value at a penetration depth, d_p.

Since the initial piston displacement represents an advancement over several axial grid locations, some procedure must be identified to "initialize" local thermal profiles into the bore surface. The Goodman integral approximation as modified by Lardner and Pohle [15] is employed. This procedure assumes that the local heat flux at each axial location is constant over the initial piston displacement. At specified axial stations the temperature distribution into the bore is represented by a parabolic profile modified by a logarithmic multiplier. The integral approximation is also used to define the initial penetration depth at each station as outlined in [15]. Since the local heat flux will vary with the incremental piston displacements to follow, the integral approximation must be abandoned for a more exact finite difference solution [16].

A finite difference solution to equation (12) is subject to the stability constraint

$$\Delta t \leq \frac{\Delta r^2}{2\alpha_D} \tag{14}$$

where Δr corresponds to an in-bore mesh spacing and Δt corresponds to a soak interval. One observes from examination of equation (14) that choosing a value of Δt (or Δr) determines the Δr (or Δt). The soak interval Δt is coupled to piston displacement as follows:

Initial displacement $\Delta t = \bar{U}_p/(L - X)$. (15a)

Incremental displacement $\Delta t = \bar{U}_p/\Delta L$. (15b)

The finite difference solution to equation (12) is implemented during the first increment piston displacement. Since the average piston velocity, $\bar{U}_p$, increases with every piston displacement, a maximum and hence permanent Δr spacing is set during the first incremental displacement. It now becomes clear why the finite difference heat conduction solution is not used during the initial piston displacement. Equation (15a) shows that the initial displacement corresponds to a large Δt which would result a very coarse grid spacing, Δr.

Axial grid spacing (ΔX) was specified prior to computation. Numerical experiments were run to determine an optimum ΔX value. The chosen value represented a trade-off between computation time (and storage demands) vs. desired accuracy. As will be shown, little advantage was eventually gained using a finer axial grid spacing with the present model.

RESULTS

Ballistic parameters used in the present study are defined in Table 2. The small tube radius and length are representative of a typical small bore system. The action cycle associated with such a system is on the order of several milliseconds. Typical ballistic performance, as expressed in terms of projectile displacement, is shown in Fig. 3. The curves show system behavior from the point of peak pressure. At this point the projectile has exhibited very little movement due to resistive forces. In actual systems such resistive force is realized as engraving of the projectile by bore rifling. The solution procedure in the present study will begin

Table 2. System input data

Initial conditions	
Piston position, L_0	1.5 in (3.81 cm)
Chamber pressure, P_0	58.0 kpsi (3.950 atm = 4.002 bar)
Gas temperature, T_0	4060°R (2255 K)
Wall temperature, $T_w(x)$	530°R (294 K)
Gas properties	
Molecular weight, M_w	24 kg/kmol
Specific heat ratio, γ	1.25
Covolume, b	0.016 ft^3/lbm (0.001 m^3/kg)
Specific heat, C_{p_m}	0.414 BTU/lbm-°R (0.414 kcal/kg-K)
Viscosity (Ref.), μ_0	1.2×10^{-4} lbm/s-ft (1.78×10^{-4} kg/m-s)
Thermal conductivity (Ref.), k_0	1.48×10^{-2} BTU/ft-hr°R (6.0×10^{-6} kcal/m-s-K)
Tube properties	
Inside radius, r_0	0.110 in (0.278 cm)
Thermal diffusivity, α_D	0.016 in^2/s (0.103 cm^2/s)
Thermal conductivity, k_s	34 BTU/ft-hr°R (0.014 kcal/m-s-K)
Piston properties	
Total travel	14.0 in (35.56 cm)
Weight, W_s	0.07 lbm (0.032 kg)

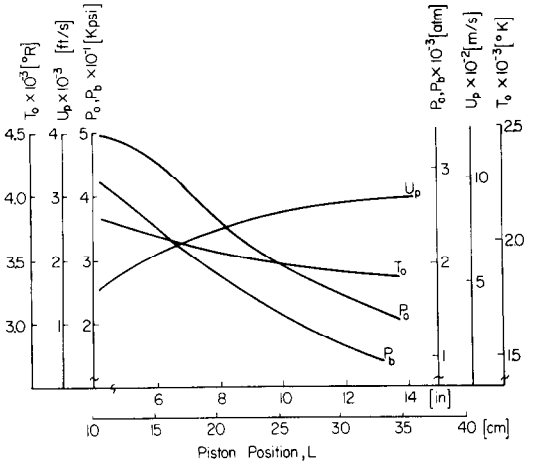

FIG. 3. Standard system performance [18].

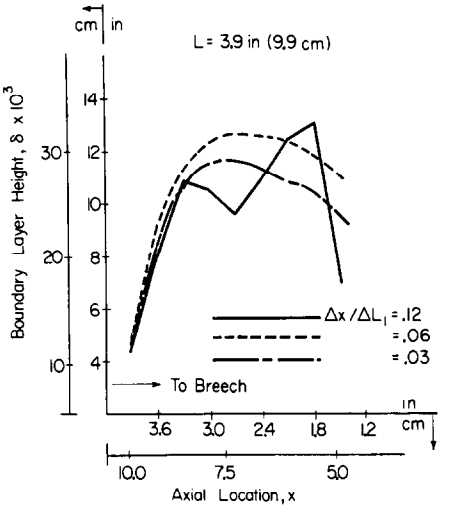

FIG. 4. Boundary layer height variation.

at the point of peak pressure. Boundary layer development at this point is assumed to be well described by conditions of streamwise and timewise similarity imposed on the present model. The error associate with this assumption is anticipated to be small in the light of the qualitative nature of subsequent comparison of computed results.

Figures 4 and 5 show the effects of axial mesh spacing. Figure 4 illustrates the sensitivity of the predicted boundary layer height (δ) to axial grid spacing. As expected, an increased number of axial locations over a fixed displacement will result in smoother predicted streamwise variation over that domain. Figure 5 illustrates that the predicted heat flux variation at the bore surface shows less sensitivity to axial grid spacing. The contrast in sensitivity of the two parameters is due in part to the somewhat nebulous manner in which boundary layer thickness is defined, namely a height where the local gas velocity achieves 99% of the local free stream value. However, accurate determination of the local boundary layer thickness becomes a significant consideration only as $\delta/r_c \geq 1$, a limit where the boundary layer assumption is no longer valid.

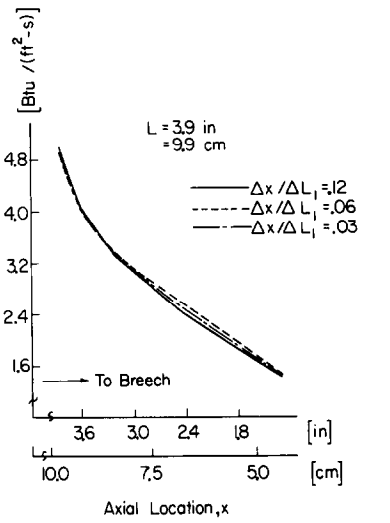

FIG. 5. Local heat flux variation.

Figure 6 exhibits the predicted boundary layer growth over several piston displacements. The shear layer thickens rapidly, representing 40% of the bore radius at a point where the piston has completed but 38% of its total travel. The current model predicts a somewhat stationary growth with the maximum thickness shifting very slowly in the direction of piston motion. The integral analyses of Shelton *et al.* [16] or Dahm and Anderson [5] predict somewhat different behavior as illustrated by Fig. 7. The results of Fig. 7 correspond to a different ballistic system than used in the present study. Projectile displacement in Fig. 7 is indicative of a large bore system which provides for significantly more time for the shear layer to develop. Large bore systems were not examined in the present study.

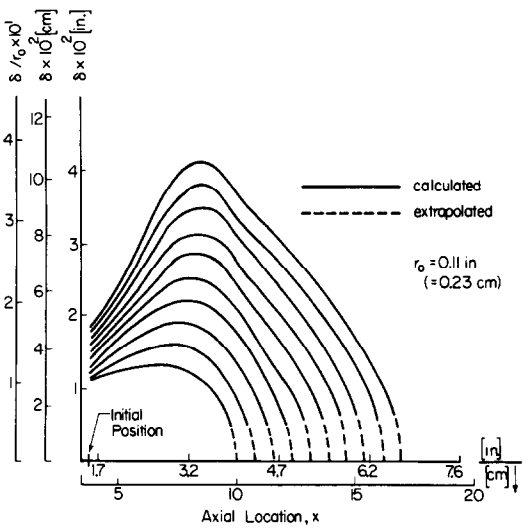

FIG. 6. Normalized boundary layer development.

Table 3 shows the results of a parametric study to determine the sensitivity of model predictions to bore curvature. As shown such influence is slight given similar ballistic performance. These results are somewhat deceiving since in actuality, one cannot arbitrarily change the bore radius without also changing ballistic performance. However, the results shown in Table 3 suggest that bore radius is perhaps a secondary consideration in boundary layer development.

Predicted variation in both the heat transfer coefficient, h_c and the bore surface temperature, T_w, are shown in Figs. 8 and 9. Figure 8 illustrates that the attenuation in the parameter h_c is quite rapid from its peak value near the piston base. However, as shown in Fig. 9, locally the parameter h_c will decrease with time. Qualitatively, the predicted trends agree with those trends observed in other studies [5, 16]. Furthermore, the predicted peak values in h_c are also of a magnitude consistent with results reported in those studies.

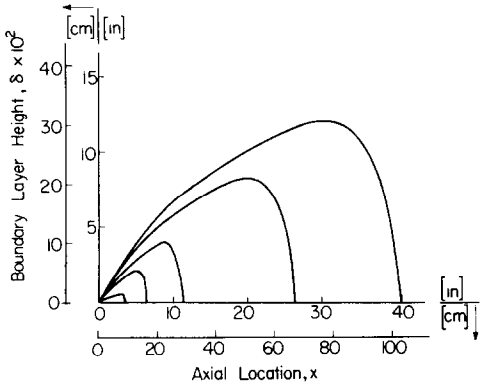

FIG. 7. Boundary layer growth: integral methods using Colburn analogy [5].

Examining Fig. 8, one observes that spatially the predicted surface temperature passes through a local maximum at any given instant in time. The dimple in the predicted temperature variation was introduced by the initialization procedure that was employed to establish the surface temperatures at new axial locations and is not representative of the real phenomenon. Figure 8 shows that the predicted local surface temperature is still increasing at a piston location corresponding to 38% of total travel. For each piston location, the present model predicts a high ($>1100°$R) but somewhat uniform variation in bore surface temperature.

The Colburn analogy

A method used in previous studies [5, 16] to relate momentum and convective heat transfer is to invoke Colburn's analogy [17] which for Prandtl numbdrs other than unity assumes the form

$$StPr^{2/3} = C_f/2, \tag{16a}$$

$$h_c = \rho_e C_p U_e St, \tag{16b}$$

where the variable St represents a local Stanton number. Equations 16(a) and (b) are generally employed as follows. The local Stanton number is defined through an empirically derived expression for the local friction coefficient, C_f. The value of C_f is expressed as a function of the local momentum thickness, θ, through the parameter Re_θ. Integral methods are employed to obtain local values for Re_θ and hence C_f. Once the local Stanton number has been defined, the local heat transfer coefficient is established using equation (16b). The above process involves a prior description of heat transfer at the bore surface which in turn will bias any calculation of shear layer development. For example, one presumes the correlation being used to determine

Table 3. Results of parametric study for variations in bore radius [ΔL = 3.0 in (= 7.62 cm)]

	*r_{0_i} = 0.11 in (= 2.79 mm)			†$r_{0_{ii}} = 5r_{0_i}$			‡$r_{0_{ii}} = 10r_{0_i}$		
	$\dot{q}$ $\times 10^{-5}$	C_f $\times 10^2$	δ $\times 10^1$	$\dot{q}$ $\times 10^{-5}$	C_f $\times 10^2$	δ $\times 10^1$	$\dot{q}$ $\times 10^{-5}$	C_f $\times 10^2$	δ $\times 10^1$
x = 4.50 in (= 11.43 cm)	0.71	0.28	0.05	0.69	0.28	0.05	0.66	0.28	0.05
x = 4.05 in (= 10.28 cm)	0.41	0.23	0.12	0.38	0.23	0.12	0.34	0.22	0.12
x = 3.45 in (= 8.76 cm)	0.26	0.21	0.18	0.26	0.21	0.18	0.24	0.21	0.18
x = 2.85 in (= 7.23 cm)	0.19	0.21	0.18	0.19	0.21	0.18	0.18	0.21	0.18
x = 2.25 in (= 5.72 cm)	0.15	0.23	0.15	0.15	0.23	0.15	0.14	0.23	0.15
x = 1.65 in	0.12	0.25	0.11	0.12	0.25	0.11	0.11	0.25	0.11

$\dot{q}$ = [BTU/ft²-s] × 2.7 = [kcal/m²-s].
* Standard system.
† Slight TVC effect.
‡ No TVC effect.

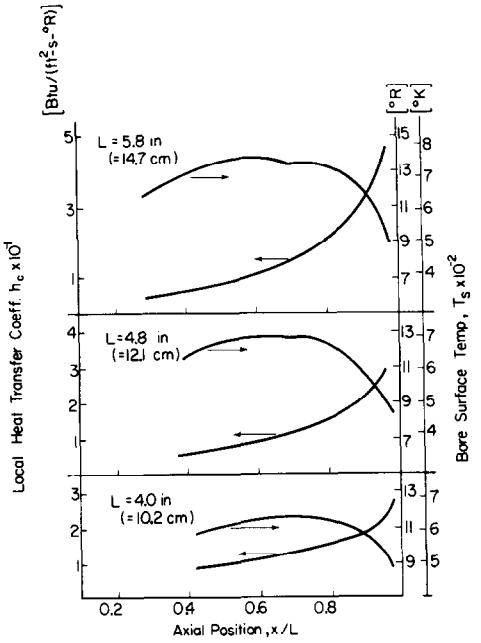

FIG. 8. Predicted heat transfer coefficient and bore surface temperature variation at different piston locations.

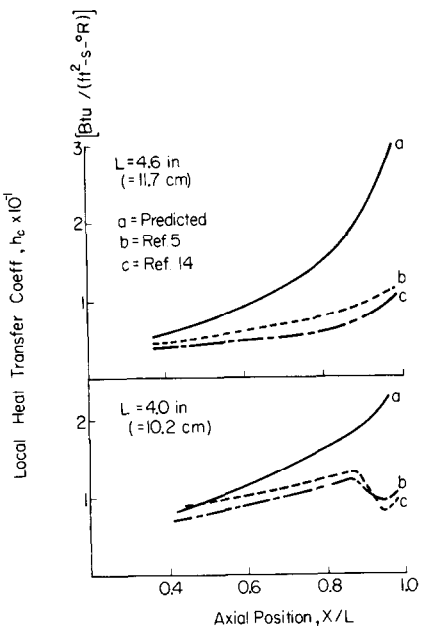

FIG. 10. Calculated vs. predicted variation in the local heat transfer coefficient.

the local friction coefficient is representative of the modeled event. Such correlations have not been accurately established for ballistic environments. The present model provides a more explicit treatment of temporal variations with the shear layer and as such is expected to provide a better approximation of the heat transfer at the bore surface.

Figure 10 shows the predicted axial variation in h_c [curve (a)] using both the present model and Colburn's analogy. As mentioned, Colburn's analogy assumes a functional form for the friction coefficient C_f. Several choices [5] [14] are reflected in the calculated variations of curves (b) and (c) in Fig. 10, namely

$$C_f = 0.0246\,(\log Re_\theta)^{-1.6}, \quad \text{curve b,} \quad (18a)$$

and

$$C_f = 0.246/[10^{0.68H} \cdot Re_\theta^{0.368}], \quad \text{curve c.} \quad (18b)$$

The Reynolds number, Re_θ, was obtained from shear layer solutions from the present model.

The present study predicts a greater axial variation

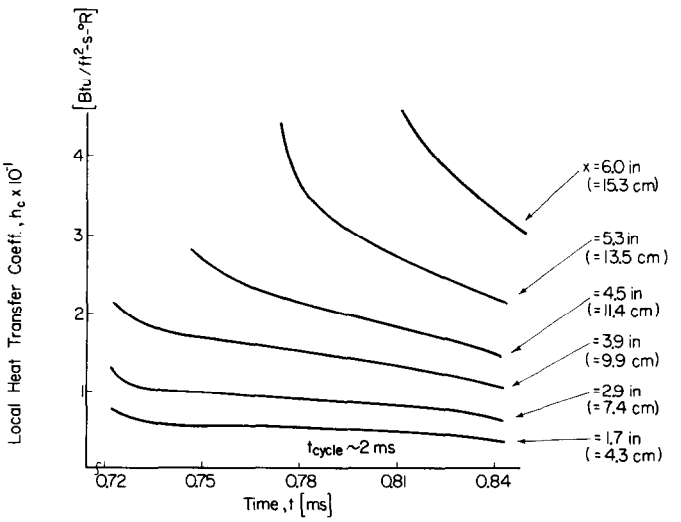

FIG. 9. Predicted temporal behavior of the local heat transfer coefficient.

in the local heat transfer coefficient, h_c. All curves indicate an attenuation in the local heat transfer coefficient with time. At a given piston displacement, Colburn's analogy appears to underestimate the local value of h_c. This suggests that bore surface temperature predictions derived using Colburn's analogy are not conservative.

CONCLUSIONS

The results just presented suggest that the following conclusions can be drawn concerning convective heating in a ballistic device.

(1) For small bore diameters, such as examined in this study, a boundary layer assumption is valid though perhaps not over the period associated with the total ballistic cycle. Shear layer development is significant for such systems and hence represents an important consideration for ballistic models which seek to predict system performance. A thin shear layer assumption is reasonable for systems employing large bore diameters.

(2) The present model shows that the local heating of the bore surface can be quite severe. Surface temperature predictions indicate such heating is most severe in the region near the breech. For the system examined in this study, the average heat flux was of the order of 10^4 BTU/ft^2-s ($\sim 3 \times 10^4$ kcal/m^2-s). Locally this average value varied by as much as a factor of 10, being largest near the piston base. The average local value of the heat transfer coefficient was approximately 20 BTU/ft^2-s-°R (~ 30 kcal/m^2-s-K). The maximum penetration distance of the thermal wave into the bore was less than one millimeter. As expected, the results indicate that a small bore system will exhibit a larger heat loss to the bore surface than large bore systems exhibiting similar performance.

(3) The often used Colburn's analogy appears to be deficient with application to the present problem of convective heating in a ballistic device. Colburn's analogy underestimates the local heat transfer coefficient. Bare surface temperature predictions are therefore not conservative.

(4) Accurate quantitative predictions of bore surface temperature using the present model will require more detailed representations of both the boundary layer turbulence near the bore surface and the inviscid core. An accurate inviscid core description is required to provide information on the spatial variation of gas properties. The present solution technique can be modified to incorporate a more descriptive core flow model in future work. Qualitatively, the predicted trends of the present study are anticipated to remain unchanged.

REFERENCES

1. M. J. Adams and H. Krier, Predicting Uniform Gun Interior Ballistics: Part II. The Interior Ballistic Code, AAE Technical Report 74-5, University of Illinois at Urbana-Champaign (1974).
2. A. C. Ajkidas, M. S. Summerfield and J. R. Ward, Reduction of gun erosion by additives, part I. Survey of wear-reducing additives, *J. Ballistics* **1**(5), 413–443 (1977).
3. A. C. Ajkidas, M. S. Summerfield and J. R. Ward, Reduction of gun erosion by additives, part II. Mechanisms of their erosion-reducing action, *J. Ballistics* **1**(5), 445–458 (1977).
4. J. R. Ward and T. L. Brosseau, Reduction of Heat Transfer to High Velocity Gun Barrels by Wear-Reducing Additives, *ASME* Paper No. 77-HT-79 (April 1977).
5. T. J. Dahm and L. W. Anderson, Propellant Gas Convective Heat Transfer in Gun Barrels, Aerotherm Report No. 70-18, Aerotherm Corporation, Mt. View, CA (28 August 1970).
6. D. L. Tuckmantel and P. C. Chou, A Computer Code to Solve the Problem of Two Phase Flow with Shocks in a Duct, BRL-CR-265, Ballistic Research Laboratories, Aberdeen Proving Ground, Maryland (October 1975).
7. A. C. Buckingham, Propellant Driven Turbulent Interior Ballistics and Wall Erosion, 17th Aerospace Sciences Meeting, Paper No. 79-007, (January 1979).
8. R. M. Kendall and E. P. Bartlett, Nonsimilar solution of the multi-component laminar boundary layer by an integral matrix method, *AIAA Jl* **6**(6) 1089–1097 (1968).
9. A. D. Anderson and T. J. Dahm, Boundary layer closure and heat transfer in constant base pressure and simple wave guns, *Trans. ASME* **100**, 690–696 (November 1978).
10. E. P. Bartlett, L. W. Anderson and R. M. Kendall, Time-Dependent Boundary Layers with Application to Gun Barrel Heat Transfer, *Proc. 1972 Heat Transfer Fluid Mech. Inst.*, Stanford University, CA (1972).
11. E. R. Van Driest, On turbulent flow near a wall, *J. aeronaut. Sci.* **23**, 1007–1011 (1956).
12. P. S. Klebanoff, Characterization of Turbulence in a Boundary Layer with Zero Pressure Gradient, NACA TN-3178 (1954).
13. T. Cebeci, A. M. O. Smith and G. Mosinskis, Calculation of compressible adiabatic turbulent boundary layers, *AIAA Jl* **8**(11), 1979–1982 (November 1970).
14. G. W. Stewart, *Introduction to Matrix Computations*. Academic Press, New York (1973).
15. T. J. Lardner and F. V. Pohle, Application of the heat balance integral to problems of cylindrical geometry, *Trans. ASME, J. appl. Mech.* **28**, 310–312 (June 1961).
16. S. Shelton, P. Saha and A. Bengles, A Study of Heat Transfer and Erosion in Gun Barrels, AFATL-TR-73-69. Air Force Armament Laboratory, Air Force Systems Command, Eglin Air Force Base, Florida (March 1973).
17. W. M. Kays, *Convective Heat and Mass Transfer*, McGraw-Hill, New York (1966).

ANALYSE DE LA COUCHE LIMITE INTERNE INSTABLE APPLIQUEE AU TRANSFERT THERMIQUE A LA PAROI DE L'AME D'UN CANON

Résumé—La convection thermique aux parois de l'ame d'un canon est d'une importance considérable quand on veut évaluer la dégradation des performances balistiques. L'objet de cette étude est d'isoler et d'examiner le chauffage convectif de façon à calculer la température de la paroi du canon pendant le tir. La structure de l'écoulement est découplée par des propriétés de coeur non visqueux avec des variations axiales et temporelles. Un modèle de mécanique des fluides est utilisé pour résoudre le développement des couches limites dynamique et d'énergie non stationnaires, compressibles et turbulentes, pour des sections fixées. Des solutions de couche à cisaillement sont couplées à travers l'équation d'énergie. On considère la conduction radiale de chaleur dans la paroi pour estimer l'évolution de la température dans la paroi en des sections à l'arrière du projectile. Les résultats, comparés aux calculs qui utilisent des méthodes intégrales et admettent connus des coefficients de transfert thermique, indiquent que les méthodes intégrales conventionnelles ne représentent pas correctement le processus convectif de la chaleur. L'influence de la courbure transverse sur le chauffage de la surface des canons étroits est étudiée. On donne des recommandations pour améliorer le présent modèle.

UNTERSUCHUNG EINER INSTATIONÄREN INNENGRENZSCHICHT—ANWENDUNG AUF DEN WÄRMEÜBERGANG IN GESCHÜTZROHREN

Zusammenfassung—Die konvektive Erwärmung von Geschützrohren ist von beträchtlicher Bedeutung für die Beurteilung der Leistungsminderung einer ballistischen Vorrichtung. Ziel dieser Studie war, die konvektive Erwärmung getrennt zu untersuchen, um die Geschützrohr-Temperatur, die während des Abfeuerns eines Geschosses auftritt, zu berechnen. Die innere Strömungsstruktur wurde durch die Spezifikation reibungsfreier Kerneigenschaften aus gemessenen und angenommenen axialen und zeitlichen Verläufen entkoppelt. Die Entwicklung der instationären kompressiblen turbulenten Reibungs- und Temperatur-Grenzschicht bei bestimmten Kolbenpositionen wurde unter Verwendung eines fluidmechanischen Modells bestimmt. Die Lösungen für die Scherströmungsschicht wurden über die Energiegleichung gekoppelt. Zur Berechnung des zeitlichen Temperaturverlaufs der Innenwand im Bereich hinter dem bewegten Geschoß wurde die radiale Wärmeleitung in die Bohrungsoberfläche berücksichtigt. Der Vergleich mit Berechnungen, die auf Integralmethoden und der Verwendung bekannter Wärmeübergangskoeffizienten beruhen, zeigt, daß herkömmliche Integralmethoden den konvektiven Wärmeübertragungsvorgang nicht hinreichend wiedergeben. Weiter wurde der Einfluß der Krümmung auf die Oberflächenerwärmung kleinkalibriger Läufe untersucht. Hinweise zur Verbesserung des vorgelegten Modells werden gegeben.

АНАЛИЗ ВНУТРЕННЕГО НЕСТАЦИОНАРНОГО ПОГРАНИЧНОГО СЛОЯ ПРИМЕНИТЕЛЬНО К ТЕПЛООБМЕНУ СТЕНОК СТВОЛА ОРУДИЯ

Аннотация — Конвективный нагрев стенок ствола орудия имеет большое значение при анализе нарушений в работе баллистического устройства. Цель данной работы заключается в том, чтобы выделить и изучить конвективный нагрев для расчёта температуры стенки ствола орудия во время поджига снаряда. Внутренняя структура течения была представлена упрощенно с помощью невязкого ядра и через измеренные и принятые осевые и временные изменения. Затем для нестационарной модели сжимаемой турбулентной жидкости были выведены уравнения пограничного слоя для импульса и энергии при дискретных положениях поршня. Уравнения пограничного слоя решались совместно с уравнением энергии. При расчёте изменения внутренней температуры стенки во времени позади двигающегося снаряда учитывалась радиальная теплопроводность. Сравнение полученных результатов с расчётами, использующими интегральные методы и известные коэффициенты теплообмена показывает, что общепринятые интегральные методы с недостаточной точностью описывают процесс конвективного теплообмена. В работе изучалось влияние поперечной кривизны на поверхностный нагрев снарядов малого калибра. Даны рекомендации по усовершенствованию настоящей модели.